Bull Math Biol
DOI 10.1007/s11538-010-9552-1

ORIGINAL ARTICLE

Evolution Stabilises the Synchronising Dynamics of Poikilotherm Life Cycles

C.A. Cobbold · J.A. Powell

Received: 10 July 2009 / Accepted: 13 May 2010

Abstract Temperature is the most significant factor controlling developmental timing of most temperate poikilotherms. In the face of climate change, a crucial question is how will poikilothermic organisms evolve when faced with changing thermal environments? In this paper, we integrate models for developmental timing and quantitative genetics. A simple model for determining developmental milestones (emergence times, egg hatch) is introduced, and the general quantitative genetic recursion for the mean value of developmental parameters presented. Evolutionary steps proportional to the difference between current median parameters and parameters currently selected for depend on the fitness, which is assumed to depend on emergence density. Asymptotic states of the joint model are determined, which turn out to be neutrally stable (marginal) fixed points in the developmental model by itself, and an associated stable emergence distribution is also described. An asymptotic convergence analysis is presented for idealized circumstances, indicating basic stability criteria. Numerical studies show that the stability analysis is quite conservative, with basins of attraction to the asymptotic states that are much larger than expected. It is shown that frequency-dependent selection drives oscillatory dynamics and that the asymptotic states balance the asymmetry of the emergence distribution and the fitness function.

Keywords Quantitative genetics · Frequency dependent selection · Evolution of phenology · Developmental rate curves

C.A. Cobbold (✉)
Department of Mathematics, University of Glasgow, University Gardens, Glasgow, G12 8QW, UK
e-mail: c.cobbold@maths.gla.ac.uk

J.A. Powell
Department of Mathematics and Statistics, Utah State University, Logan, UT 84322-3900, USA
e-mail: powell@math.usu.edu

Published online: 09 June 2010

1 Introduction

Contemporary populations face historically unprecedented rates of environmental alteration, including habitat changes, species introductions, and global climate change (Chesson and Huntly 1997) that may substantially affect global diversity as well as distribution and abundance of natural resources. Thomas et al. (2004) predict, purely on ecological considerations, that 15–37% of species in their study areas face extinction as a direct consequence of global warming. Climate change will have particular impact on poikilotherms, since temperature drives life history events (phenology) in these organisms. Insects, and especially eruptive insects, may become the primary agents of large-scale ecological change in an era of climate warming (Logan et al. 2003).

Long-term persistence of populations in changing environments depends on their ability to disperse to suitable environments, respond via phenotypic plasticity, or adapt (Holt 1990). The rate and trajectory of adaptation is limited by the genetic architecture of traits under selection. Recent focus on understanding limits of adaptation in changing environments has resulted from empirical and conceptual advances. First, there is growing recognition that evolution and adaptation occur over ecologically relevant time scales (Thompson 1998; Hendry et al. 2000; Reznick and Ghalambor 2001). Second there is increasing emphasis on incorporating evolutionary parameters into demographic models. Combined approaches are useful in modelling extinction probabilities in changing environments (Lynch and Lande 1993; Gomulkiewicz and Holt 1995) and in theoretical treatments of evolution of species interactions (Johnson and Agrawal 2003). The basic idea is to treat a parameter in a deterministic demographic model as a heritable trait which can change from generation to generation in response to selective pressure. A fitness function (per capita growth rate for individuals with the particular trait) must be determined, and the selective pressure on the trait can then be determined from the distribution of trait values and the fitness function. While these studies have been illuminating, and underscore the importance of including evolutionary perspectives in quantitative understandings of species abundance and dispersion, the link between adaptation and warming is weak because the evolving traits have no direct connection to climate variables.

In this paper, we will outline how a well-established model for insect phenology can be connected with a quantitative genetic approach to the evolution of phenological traits. The traits under selection control the rates of development in demographic models for life cycle timing in insects (see Powell and Logan 2005 for a review). Temperature has a direct and explicit role, controlling the timing of life history events including oviposition, egg hatch, pupation, and emergence of adults, allowing climatic variables to be tied directly to the number of (surviving) offspring produced per adult (i.e. fitness). Variability in developmental rate is represented by a distribution of parameters across the population within a generation. Since differing traits produce differing emergence times and, therefore, differing fitness values, the mean trait value changes from generation to generation according to a quantitative genetic recursion. Evolution of phenology under the proximal influence of temperature occurs at a rate depending on the heritability of the trait and the variance of its distribution according to the univariate breeder's equation. As fitness relies on synchronised emergence of

individuals, selection in this model takes the form of frequency-dependent selection, and thus the fitness landscape in the model evolves. This is in contrast to frequency-independent selection where the fitness landscape remains unchanged.

We also characterize the attracting states of the model. The temporal dynamics of phenology by itself are organized by fixed points of a circle map of emergence dates on a cyclic domain of seasonal days, as will be reviewed in the first section below. The evolution of median phenological parameters change the location of this fixed point from generation to generation for most of the population, ultimately leading to a state which would be only marginally stable in the context of the phenological model alone. Asymptotic dynamics are examined using steepest descents, and results confirmed and explored numerically.

2 Modelling Phenology and the Evolution of Heritable Parameters

We begin by briefly reviewing phenology models, so that the influence of rate parameters (the traits under evolution) on life cycle timing (the phenotype under selection) can be understood.

2.1 Developmental Timing with Direct Temperature Control

Deterministic models of the relationship between environmental variables, particularly temperature, and developmental timing (phenology) are based on the notion of relating the rate of progress through a life stage to empirical rate functions. For organisms under direct temperature control (that is, lacking diapause or other physiological timing mechanisms (Danks 1987)), this results in a particularly simple mathematical approach. Let $a_j(t)$ denote the fraction of development toward completion which has occurred in life stage j by time t. Then

$$\frac{da_j}{dt} = R_j\big(T(t)\big), \tag{1}$$

where R_j is the rate of development for stage j, which depends on environmental temperature $T(t)$. Developmental milestones are those times, t_j, at which one life stage terminates and another begins, generally associated with observable developmental events (the hatching or laying of eggs, or larval molts). Thus, (1) has initial condition $a_j(t_{j-1}) = 0$, indicating that an organism begins life stage j immediately on termination of the previous stage.

Equation (1) can be solved by integrating

$$a_j(t) = \int_{t_{j-1}}^{t} R_j\big(T(\tau)\big)\, d\tau. \tag{2}$$

Given one developmental milestone, t_{j-1}, the next milestone, t_j, is determined implicitly,

$$1 = a_j(t_j) = \int_{t_{j-1}}^{t_j} R_j\big(T(\tau)\big)\, d\tau. \tag{3}$$

While the original equation is simple, in most cases t_j is a nonlinear function of t_{j-1}, filtered through the nonlinear dependence of developmental rate on temperature and the complicated dependence of temperature on time.

Suppose an insect completes its life cycle in N stages, beginning with eggs in stage 1 and terminating with egg-laying (oviposition) in stage N. Let t_0^n denote the oviposition date in generation n. Given temperatures and rates for a particular organism, the timing of life-history events can be calculated using (3), giving a sequence of dates $t_0^n, t_1, \ldots, t_{N-1}, t_N = t_0^{n+1}$. Since t_N denotes the end of one generation and the beginning of another, and is a deterministic function, G, of t_0^n, we can write

$$t_0^{n+1} = G\left(t_0^n\right). \tag{4}$$

The G-function encapsulates the deterministic relationship between environmental temperatures and developmental timing.

As discussed by Powell and Logan (2005), the stable fixed points and attracting orbits of G, modulo one or more years, organize the distribution of emergence and oviposition for a population. Assuming that all individuals have the same rate curves and parameters, it can be shown that emergence dates for the entire population will be attracted to an orbit of oviposition dates on the periodic cycle of Julian days from 1 to 365. The *voltinism* of a population is the number of generations completed (on average) in a year, and is equivalent to the winding number of the G-function map for a given, periodic temperature signal.

Of particular interest for temperate insects are univoltine (one generation per year) fixed points, for which the life cycle is locked to the seasonal temperature cycle. This amounts to the intersection of the graph of $G(t)$ and the line $t + 365$ (see Fig. 1). The attracting orbit, in this case, is simply one or more stable fixed points, which synchronize the population (thus improving chances of finding mates, lowering per-capita predation) as well as time critical life stages (so that, for example, cold-hardened or drought-resistant stages emerge at appropriate times of year, or are timed to occur during the presence of resources). The advantage of having an integral number of life stages per year is so great that many insects have evolved specific physiological mechanisms, in particular diapause (Zaslavski 1996) to maintain integral voltinism. However, diapause generally limits an organism to geographic regions where the signals controlling its inception and breaking are seasonally appropriate. Accordingly, many organisms do not exhibit diapause, and are therefore said to be under direct temperature control (Danks 1987). In the case of direct temperature control, seasonal variation of temperatures and nonlinear dependence of developmental rates on temperatures is sufficient to establish integral voltinism (see Jenkins et al. 2001; Powell et al. 2000).

The purpose of this paper is to use the quantitative genetic formalism for the evolutionary response of phenotype to determine the evolutionary stability of direct temperature control as a timing mechanism. We will treat specific rate curve parameters as quantitative traits, filter the fitness of individuals through emergence days predicted by the G-function, and use this to predict shifts in the parameters controlling the developmental rate curves. This establishes a mechanism with which to determine how (and if) populations can adapt to climate change or novel thermal environments.

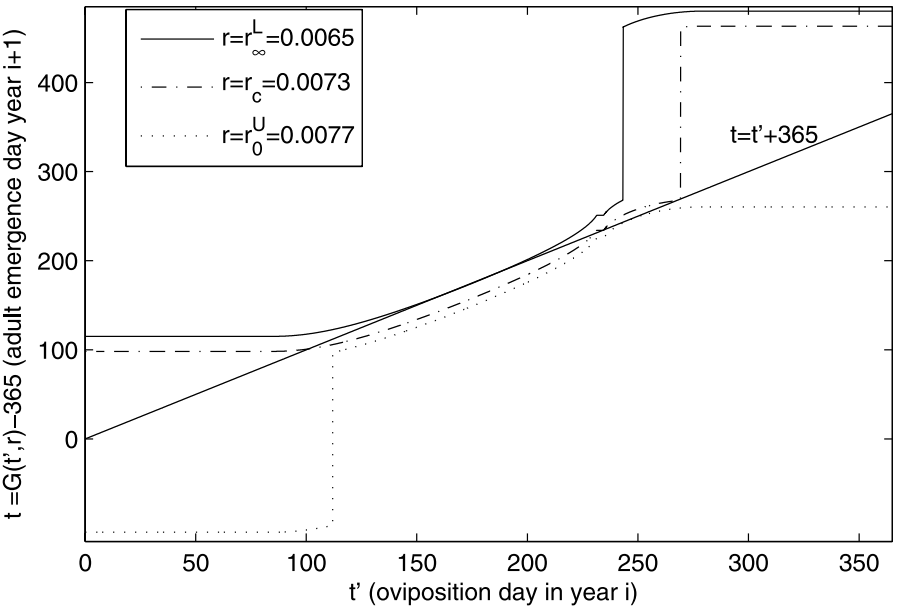

Fig. 1 Illustration of the phenology model, $t_{i+1} = G(t_i, r)$, for 3 values of r. As r increases, the G function shifts down the vertical axis. For sufficiently large r, the characteristic shape of the G function changes, the vertical jump discontinuity switches location (compare $r = 0.0073$ and $r = 0.0077$). The *solid curve* $r = r_0^L = 0.0065$, gives a G function with a marginal fixed point located early in the year, the lower marginal fixed point. The *dash-dot curve*, $r = 0.0073$, gives a G function with two stable fixed points. The *dotted curve* $r = r_0^U = 0.0077$, gives a G function with a marginal fixed point located late in the year, the upper marginal fixed point

While the evolutionary model we outline works for any G-function, the specific case considered in detail here will be the two-stage, four parameter phenology model

$$R_1\big(T(t)\big) = \begin{cases} 0, & T < \theta_1, \\ \rho_1(T - \theta_1), & T \geq \theta_1, \end{cases} \quad \text{and} \quad R_2\big(T(t)\big) = \begin{cases} 0, & T < \theta_2, \\ r, & T \geq \theta_2, \end{cases} \tag{5}$$

introduced by Powell et al. (2000) and discussed in detail in Powell and Logan (2005). This basic model has the features often observed in insect phenology, including differing developmental thresholds for different life stages (θ_1 and θ_2), linear developmental dependence on temperature above some threshold in some stages (as in a 'degree-day' model) and constant developmental rate above threshold in other stages (as in 'feeding' stages, where development is eating to gain weight before emerging). In the presence of simple, periodic temperatures,

$$T(t) = T_0 - T_1 \cos\left(\frac{2\pi t}{365}\right), \tag{6}$$

(with yearly mean temperature T_0, seasonal change of $T_1 - T_0$ from January 1 (day 1) to June 29 (day 365/2)) the model can exhibit univoltine fixed points in nontrivial open sets of all four parameters (Powell and Logan 2005).

2.2 The Evolution of Developmental Rate Using Quantitative Genetics

Understanding the evolution of developmental rate is crucial to examining the effects of temperature increases synonymous with global warming and climate change. We employ quantitative genetics (Lande 1976) to study the evolution of a quantitative trait, r, the rate parameter in (5). Later we discuss numerical evidence that our results continue to hold for the remaining rate curve parameters, θ_1, θ_2, and ρ_1.

The population is assumed to have discrete nonoverlapping generations. We increment the model yearly, on January 1, when temperatures are low enough that development is arrested in all life stages. The mean developmental rate in year $n+1$, $\bar{r}_{n+1}$, is calculated using the Univariate Breeder's Equation (UBE) (Lande 1976)

$$\Delta\bar{r} = \bar{r}_{n+1} - \bar{r}_n = \underbrace{\Big(\overbrace{\bar{r}_{\text{selection}}}^{\substack{\text{Mean } r \text{ after selection}\\ \text{before reproduction}}} - \overbrace{\bar{r}_n}^{\substack{\text{Mean } r \text{ before selection}\\ \text{and reproduction}}}\Big)}_{\text{Selective force in generation } n} \underbrace{h^2}_{\substack{\text{Realised}\\ \text{heritability}}}. \tag{7}$$

The background assumption is that r is normally distributed in the population according to

$$p(r) = \frac{1}{\sqrt{2\pi\sigma^2}} \exp\left(\frac{-(r-\bar{r})^2}{2\sigma^2}\right).$$

The mean, $\bar{r}$, is subject to evolution while the variance, σ^2, is fixed. The heritability parameter, h^2, is the ratio of genetic to total phenotype variances, and measures the fraction of phenotype variability which can be passed from one generation to the next. Rearranging (7) gives the following recursion relation for $\bar{r}_n$,

$$\bar{r}_{n+1} = \bar{r}_n + h^2(\bar{r}_{\text{selection}} - \bar{r}_n). \tag{8}$$

The mean after selection, $\bar{r}_{\text{selection}}$, is weighted by the fitness, $W_n(r)$, or per capita growth rate of individuals with rate parameter r,

$$\bar{r}_{\text{selection}} = \frac{1}{\overline{W}_n} \int_{r\in\mathbb{R}} r\, W_n(r)\, p(r)\, dr, \tag{9}$$

where $\overline{W}_n = \int_{r\in\mathbb{R}} W_n(r)\, p(r)\, dr$. The fitness of each r describes the strength and direction of selection.

Fitness depends on the number of individuals completing development to emerge as adults at the same time, t, as this determines the number of offspring produced. We assume that only individuals emerging at the same time can mate, mating is random, and oviposition occurs at the time of mating. A more realistic assumption is that individuals mate over several days; however, if the mean value for r prior to reproduction is the same on each of these days then these two mating strategies are equivalent in terms of phenotype evolution. Figure 2 illustrates that broadly the mean is the same on each day and only those emerging on day 125 have a mean r that is high, but the mode phenotype is in line with the rest of the population. Additionally, the UBE as-

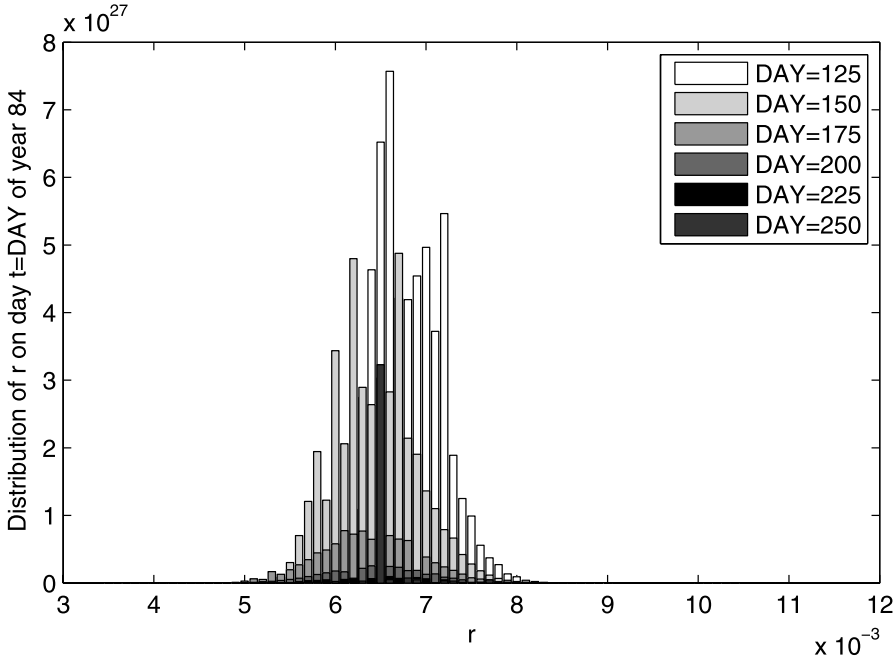

Fig. 2 Plot of the distribution of r upon emergence as adults ($A_n(t)$), but prior to reproduction on days $t = 125$, 150, 175, 200, 225, and 250 in year 84. The mean developmental rate of each day is similar indicating that it is a reasonable assumption to say that r following reproduction will be distributed in the same way on each day. The model parameters used are as given in the main text and Fig. 6 illustrates the emergence distribution corresponding to this year

sumes that reproduction results in the quantitative trait r being normally distributed in the population, with mean $\bar{r}_{n+1}$. When the trait is controlled by several loci, each of which having a relatively small effect, such an assumption is valid (Slatkin 1980). Taylor's (1981) study of developmental rate curves for 54 insect species provides further support for the normality assumption.

We specify a fecundity function which depends linearly on the density of emerging adults, reflecting the increased likelihood of finding mates and successfully producing brood. Adults emerging at a given time, t, may have a range of phenotypes and oviposition dates. To specify fitness for a particular phenotype requires determining what fraction of individuals with phenotype r, starting as eggs *this* year, emerge *next* year, and successfully produce brood according to a fecundity function. First, the dependence of emergence time on both phenotype and starting time (i.e. the G function) must be inverted. Secondly, holding rate (r) fixed, fecundities must be integrated across all days of emergence to determine total offspring produced by individuals sharing the same parameter. Divided by the total number of individuals with that parameter gives the fitness (surviving offspring/parent) for the subpopulation with parameter r. This fitness then drives the UBE.

To calculate the date of developmental completion, we use the two life-stage phenology model described in Sect. 2.1. An egg oviposited on day t' of year n, with de-

velopmental rate r, will complete development on day $G(t', r)$. Thus, an adult with rate r emerging on day t will develop from an egg laid on day $G^{-1}(t, r)$. Semivoltine (taking 2 years to develop) or bivoltine (two generations per year) individuals are removed from the population under the assumption that they have an inappropriate seasonality. For example, mortality is high for semivoltine individuals because they must survive two winters, while bivoltine individuals are likely to emerge late in the year when conditions for offspring survival are unfavourable.

We denote the distribution of eggs in year n by $E_n(t')$, where t' is the date in year n. The emergence of adults in the next year, with density $A_{n+1}(t)$, depends on $E_n(t')$ and the (t', r) pairs that give emergence on day $t = G(t', r)$. Assuming 100% developmental survivorship and noting that $t' = G^{-1}(t, r)$ and $dt' = dt/G_t(t, r)$, there are $E_n[G^{-1}(t, r)]\frac{dt}{G_t(t,r)}\,p(r)\,dr$ adults emerging on day t of year $n + 1$ with developmental rate r. We now drop the prime for convenience. We can now calculate the total density of adults emerging on day t of year $n + 1$, denoted by $A_{n+1}(t)$, as follows:

$$A_{n+1}(t) = \int_{-\infty}^{\infty} \underbrace{E_n\big[G^{-1}(t, r)\big]\frac{p(r)\,dr}{G_t(t, r)}}_{\substack{\text{Density of adults of type } r \\ \text{emerging on day } t}}. \tag{10}$$

We illustrate the mapping of an initial egg distribution, E_n, to the adult distribution in Fig. 3.

To calculate fitness, $W_n(r)$, or per capita growth rate of individuals with developmental rate r, we define $\lambda_{n+1}(t, r)$, the density of eggs produced on day t of year $n + 1$ by parents with rate parameter r, and write

$$\lambda_{n+1}(t, r) = \overbrace{f\big(A_{n+1}(t)\big)}^{\substack{\text{Total density of eggs} \\ \text{laid on day } t \text{ of year } n+1}} \quad \frac{\overbrace{E_n\big[G^{-1}(t, r)\big]\frac{p(r)}{G_t(t,r)}}^{\substack{\text{Proportion of emergers on day} \\ t \text{ which developed at rate } r}}}{A_{n+1}(t)}. \tag{11}$$

Here, f is a functional response describing reproductive success of the adults. Examples of f include a type I response, reflecting a linear increase of reproductive potential with density (as in increased chances of finding a mate). A type III response models an Allee effect, whereby populations must exceed a threshold density before successful reproduction is possible (as when high densities may be necessary to overcome a hosts defenses). For simplicity, we will use a type I response,

$$f\big(A_{n+1}(t)\big) = kA_{n+1}(t), \tag{12}$$

where k is the average number of surviving offspring produced per adult female. The fitness, $W_n(r)$, can then be found by integrating $\lambda_{n+1}(t, r)$ over t, and dividing by the

number of parents (eggs oviposited in year n with developmental rate parameter r);

$$W_n(r) = \frac{\overbrace{\int_0^\infty \lambda_{n+1}(t,r)\,dt}^{\substack{\text{Total density of eggs produced in year} \\ n+1 \text{ laid by parents with rate parameter } r}}}{\underbrace{\int_0^\infty E_n(t)\,p(r)\,dt}_{\substack{\text{Total number of eggs laid in year } n \text{ that developed with rate} \\ \text{parameter } r \text{ to become the parents of eggs laid in year } n+1}}}. \tag{13}$$

While complicated, this formalism provides all the ingredients necessary to evaluate $\bar{r}_{\text{selection}}$ in the UBE, and thus calculate how evolution of the trait changes the median parameter, $\bar{r}_n$, from generation to generation.

The distribution of individuals must also change from year to year, since both differing dates and differing rates translate into differing fecundities. To complete the model, we define a map describing the change in egg density from year to year, given by

$$E_{n+1}(t) = f\big(A_{n+1}(t)\big) = k\,A_{n+1}(t) = k\int_{-\infty}^{\infty} E_n\big[G^{-1}(t,r)\big]\frac{p(r)\,dr}{G_t(t,r)}. \tag{14}$$

The complete model is given by (8) and (14) and consists of the quantitative genetics recursion for the mean developmental parameter ($\bar{r}_n$) and the egg distribution ($E_n(t)$), respectively. In Sect. 3, we characterize the attracting states of this recursion.

3 Analytic Results

3.1 Determining Fixed Points

We begin with an analytic characterisation of the asymptotic parameter value r_0, the attracting state of (8). Developmental rates are distributed normally as

$$p(r) = \frac{1}{\sqrt{2\pi\sigma^2}} e^{-\frac{(r-\bar{r})^2}{2\sigma^2}}. \tag{15}$$

If r is a true rate, that is, the inverse of development time, then noting $dr = -t^{-2}\,dt$ gives a distribution of emergence events,

$$t^{-2}p\big(t^{-1}\big) = \frac{1}{t^2\sqrt{2\pi\sigma^2}} e^{-\frac{(t^{-1}-\bar{r})^2}{2\sigma^2}} = \frac{1}{t^2\sqrt{2\pi\sigma^2}} e^{-\frac{(t-t^*)^2}{2t^2t^{*2}\sigma^2}}. \tag{16}$$

Here, we take $t^* = \bar{r}^{-1}$ as the peak time of emergence. The shape of this distribution, and its consequences for the emergence of a life stage, are discussed in Gilbert et al. (2004).

The quantitative genetic recursion for the median rate can only converge if the emergence distribution ($E_n(t)$) also converges. A fixed point analysis therefore requires that we account for the shape of the emergence profile, $E_n(t)$. We make the

ansatz that only one parameter, r, evolves, since r is inversely proportional to developmental time above the second threshold, θ_2. Extension to the evolution of other parameters requires only including the explicit dependence of rate on the parameter under consideration (and temperature). We further assume that there is no variation in other developmental parameters and, therefore, think of the distribution of emergence for the entire developmental map as being approximated by

$$E_n(t) = \frac{N}{t^2\sqrt{2\pi\sigma^2}} e^{-\frac{(t-t_n^*)^2}{2t^2 t_n^{*2}\sigma^2}}. \tag{17}$$

Here, N is the total number of adults emerging, and we take t_n^* to be located at the stable univoltine fixed point of the G-function, calculated for the current median parameter, $\bar{r}_n$. This fixed point varies from generation to generation as $\bar{r}_n$ evolves, but to simplify notation we will simply take $t^* = t_n^*$.

Now we substitute these forms into the genetic recursion relation (8) and determine the parameter values corresponding to fixed points. In the case of a type I functional response, $f(A_{n+1}(t)) = kA_{n+1}(t)$ and the fitness becomes

$$W_n(r) = \frac{\int_0^{365} E_n[G^{-1}(t,r)]\frac{k}{G_t}\,dt}{\int_0^{365} E_n(t)\,dt}. \tag{18}$$

Noting that the combination of G^{-1} and $1/G_t$ in the integrand amounts to a change of variables, and taking the integral to 365 as an approximation to ∞, we may write the average fitness as

$$\bar{W}_n = k \tag{19}$$

and thus

$$\bar{r}_{\text{selection}} = \frac{1}{k}\int_0^\infty k \underbrace{\int_{-\infty}^{\infty} rp(r)E_n\big[G^{-1}(t,r)\big]\frac{1}{NG_t}\,dr}_{\spadesuit(t)}\,dt. \tag{20}$$

The $\spadesuit(t)$ term will be evaluated using steepest descents, noting that $t^*(r)$ is a function of r and using a linear approximation for G^{-1},

$$G^{-1}(t,r) \approx t^* + \frac{(t-t^*)}{G_t^*},$$

since $G^{-1}(t^*,r) = t^*$ and the slope of the inverse is $G_t^{-1}(t^*,r) = 1/G_t^*$. The approximation is valid provided the G-function has relatively shallow curvature, an assumption discussed below. We write

$$\spadesuit(t) = \int_{-\infty}^{\infty} \frac{re^{s(t,t^*,r,\bar{r})}}{G_t(t,r)t^2 2\pi\sigma^2}\,dr, \tag{21}$$

with

$$s = -\frac{1}{2\sigma^2}\left[(r-\bar{r})^2 + \frac{(t-t^*)^2}{t^{*2}[t+(G_t^*-1)t^*]^2}\right]. \tag{22}$$

To find the stationary point, we look for r such that

$$0 = \frac{\partial s}{\partial r} = \frac{-(r-\bar{r})[(G_t^*-1)t^*+t]^3 t^{*3} - \frac{\partial t^*}{\partial r}[t^3 + t^2 t^*(2G_t^*-3) - 3tt^{*2}(G_t^*-1) + t^{*3}(G_t^*-1)]}{\sigma^2 t^{*3}[t+(G_t^*-1)t^*]^3}. \tag{23}$$

In principle, this defines a stationary point, $r = \hat{r}$, so that the integral in (20) can be evaluated asymptotically. The stationary point defined by (23) is

$$\hat{r} = \bar{r} + \frac{\partial t^*}{\partial r}\frac{t^3 + t^2 t^*(2G_t^*-3) - 3tt^{*2}(G_t^*-1) + t^{*3}(G_t^*-1)}{t^{*3}[(G_t^*-1)t^*+t]^3}. \tag{24}$$

The asymptotic form of (21) is then given by

$$\spadesuit(t) \sim \sqrt{\frac{2\pi}{-s_{rr}(t,t^*,\hat{r},\bar{r})}}\frac{\hat{r}e^{s(t,t^*,\hat{r},\bar{r})}}{G_t(t,\hat{r})t^2 2\pi\sigma^2}. \tag{25}$$

We note that, since the combination of G^{-1} and $\partial_t(G^{-1}) = 1/G_t$ amounts to a change of variables in time in (20) and $\int E_n(t)\,dt = N$, at leading order the $\bar{r}_{\text{selection}}$ generated by steepest descents is precisely the stationary point, that is, $\bar{r}_{\text{selection}} = \hat{r}$. Thus, the first requirement for a fixed point becomes $\bar{r} = \hat{r}$, so that the evolutionary dynamics are stationary in the UBE (8). Consequently, $\frac{dt^*}{dr} = 0$ to satisfy (24).

The asymptotic form of $\spadesuit(t)$ in (25), is the predicted emergence distribution over days of the year, which must be in direct proportion to the emergence *ansatz*, (17), in order for the shape of the distribution to be stationary. This amounts to requiring

$$s\big(t, t^*(\hat{r}), \hat{r}, \bar{r}\big) = -\frac{(t-t^*)^2}{2\sigma^2 t^{*2} t^2}. \tag{26}$$

Evaluating s at the stationary point gives

$$s = -\frac{(t-t^*)^2}{2\sigma^2 t^{*2}[t+(G_t^*-1)t^*]^2}. \tag{27}$$

Comparing expressions (26) and (27) it is apparent that

$$G_t^* = 1$$

to ensure that the shape of the emergence distribution is stationary. This means that the slope of the G function at the asymptotic fixed point for the evolutionary dynamics is only marginally stable with respect to purely phenological dynamics.

3.2 Stability Analysis

Given that a necessary condition for existence of an equilibrium distribution is tangential intersection (and, therefore, marginal stability of the dynamics of emergence

time when parameters are fixed and $\sigma = 0$), it is important to ask if such a distribution can be stable in the context of evolutionary dynamics. We give a stability analysis in this section under idealized circumstances to illustrate the basic stability requirements and highlight some of the technical difficulties. We will assume that the marginal fixed point is located at a saddle-node bifurcation for fixed points in emergence time, where r is the bifurcation parameter, that these are the only two fixed points for G and that the time separation between the bifurcating stable/unstable points is large relative to the duration of the emergence distribution (i.e. $\sigma t_0 \ll 1$). Additionally, we will idealize the situation so that there is no loss of individuals who fail to complete development in a year (or complete before the beginning of a new year). These simplifications mean that the stability analysis given here will not correspond precisely to observations in the numerical case studies later in this paper, but will only indicate basic trends. The numerical case studies require loss of nonunivoltine individuals (which tends to stabilize the distribution) as well as use of the two-stage phenology model above (which can have more than two fixed points in some parameter regimes).

Let r_0 be the parameter at which the G function has a marginal, tangential fixed point and t_0 the location of that fixed point in Julian days. We seek to determine how $\bar{r}_n$ will evolve when it is 'close' to its asymptotic state, r_0. Stability analysis of the distributional recursion for $E_n(t)$ and $\bar{r}_n$ is an infinite dimensional problem. However, the smaller the breadth, σ, of the distribution of parameters the closer the dynamics become to a simple recursion in the median rate, with parameters in the recursion determined by steepest descents evaluations of the integrals in (20) as the variables are perturbed from their equilibrium values.

We first introduce an approximation to the shape of G and use it to determine appropriate scales for the stability analysis. Using the marginality condition ($G(t_0, r_0) = t_0$ and $G_t(t_0, r_0) = 1$), near the equilibrium state and a Taylor expansion,

$$G(t', r) \simeq t_0 - \gamma^2 t_0^2 (r - r_0) + (t' - t_0) + \alpha^2 \frac{1}{t_0}(t' - t_0)^2, \tag{28}$$

where

$$\gamma^2 = -\frac{1}{t_0^2}\frac{\partial G}{\partial r}(t_0, r_0), \qquad \alpha^2 = t_0 \frac{1}{2}\frac{\partial^2 G}{\partial t^2}(t_0, r_0) \tag{29}$$

and α and γ are dimensionless. Equation (28) can be solved explicitly for G^{-1},

$$t' = G^{-1}(t, r) = t_0 \frac{2\alpha^2 - 1}{2\alpha^2} + \frac{t_0}{\alpha}\left[\frac{t}{t_0} + \frac{1}{4\alpha^2} - 1 + t_0 \gamma^2 (r - r_0)\right]^{\frac{1}{2}}. \tag{30}$$

Solving $t^*(r) = G(t^*(r), r)$ gives

$$t^* = t_0 \pm \frac{\gamma}{\alpha} t_0^{\frac{3}{2}} \sqrt{r - r_0}. \tag{31}$$

Of these two the negative root corresponds to the stable, univoltine emergence date.

The root dependence of $t^*(r)$ on $r - r_0$ suggests the proper scaling to use for the stability analysis. We define the order parameter, $\epsilon = \sigma t_0$ (so that the emergence

distribution will be narrow) and introduce rescaled variables for r near r_0 and small perturbations, δ_n, of the current mean phenotype, where

$$\bar{r}_n - r_0 = \epsilon^2 \frac{1}{t_0} \bar{\delta}_n^2 \quad \text{and} \quad r - r_0 = \epsilon^2 \frac{1}{t_0} \delta^2.$$

Thus,

$$t^*(r) = t_0 \left(1 - \epsilon \delta \frac{\gamma}{\alpha} \right).$$

The variable t is also involved through the distribution $E_n(t)$ and the integration (20) which determines $\bar{r}_{\text{selection}}$ in each generation; we can choose a simple scaling for time,

$$t = t_0(1 + \epsilon\tau),$$

and proceed to determining the asymptotic behaviour of $\spadesuit(t)$ in these scaled variables using the method of steepest descents.

The first step will be to determine the location of the critical point of (22) in δ. Let the critical point, $\hat{\delta}$, be expanded in an asymptotic series

$$\hat{\delta} = \hat{\delta}_0 + \epsilon^2 \hat{\delta}_1 + \cdots.$$

The derivative of the exponent, (22), becomes

$$\frac{\partial s}{\partial r} = \frac{1}{\epsilon^2} \left[s_0(\hat{\delta_0}, \tau) + \epsilon^2 s_1(\hat{\delta_0}, \hat{\delta_1}, \bar{\delta}_n, \tau) + O\left(\epsilon^4\right) \right].$$

This generates a system of equations

$$s_0 = -\frac{\gamma t_0}{2\hat{\delta_0}\alpha^2} \left(\gamma \hat{\delta}_0 + \alpha\tau \right) = 0, \tag{32}$$

giving $\hat{\delta}_0 = -\frac{\alpha}{\gamma}\tau$, and

$$s_1\left(\hat{\delta}_0, \hat{\delta}_1, \bar{\delta}_n, \tau\right) = \frac{t_0}{2\tau\alpha^3} \left(2\tau\alpha^3 \bar{\delta}_n^2 - 2\tau^3 \frac{\alpha^5}{\gamma^2} + \gamma^3 \hat{\delta}_1 \right) = 0. \tag{33}$$

We note that odd powers of epsilon in the asymptotic expansions vanish and so do not appear above.

Solving (33) gives

$$\hat{\delta}_1 = 2\tau \frac{\alpha^3}{\gamma^3} \left(\frac{\alpha^2}{\gamma^2}\tau^2 - \bar{\delta}_n^2 \right).$$

An asymptotic expansion for the stationary point, $\hat{r}$, is

$$\hat{r} = r_0 + \epsilon^2 \frac{1}{t_0} \hat{\delta}^2 = r_0 + \epsilon^2 \frac{\alpha^2\tau^2}{\gamma^2 t_0} \left[-1 - 2\epsilon^2 \frac{\alpha^2}{\gamma^2} \left(\bar{\delta}_n^2 - \frac{\alpha^2}{\gamma^2}\tau^2 \right) + \cdots \right]^2. \tag{34}$$

The second derivative at the stationary point is

$$s_{rr} = -\frac{t_0^2\gamma^4}{4\alpha^4\tau^2\epsilon^4}\big(1-4\epsilon\tau\big(1+\alpha^2\big)+O\big(\epsilon^2\big)\big).$$

Then the steepest descents theorem gives (after some symbolic manipulation of (25))

$$\spadesuit(t) \sim e^{q(\tau,\bar{\delta}_n)}\frac{r_0|\tau|\alpha^2}{t_0\gamma^2}\sqrt{\frac{2}{\pi}}\left[1-\epsilon^2\frac{\alpha^2}{\gamma^4}\left(5\alpha^2\tau^2-3\gamma^2\bar{\delta}_n^2-\frac{\gamma^2\tau^2}{r_0t_0}\right)+O\big(\epsilon^4\big)\right], \quad (35)$$

where the exponent at the critical point, $q(\tau,\bar{\delta}_n)$, is

$$q(\tau,\bar{\delta}_n) = -\frac{\epsilon^2}{2\gamma^4}\left[\big(\alpha^2\tau^2-\gamma^2\bar{\delta}_n^2\big)^2-4\alpha^4\tau^2\frac{\epsilon^2}{\gamma^4}\big(\alpha^2\tau^2-\gamma^2\bar{\delta}_n^2\big)^2+O\big(\epsilon^4\big)\right]. \quad (36)$$

To determine $\bar{r}_{\text{selection}}$, we still have another integration to accomplish,

$$\bar{r}_{\text{selection}} = \int_0^\infty \spadesuit(t)\,dt \sim \epsilon t_0\int_{-\infty}^{\infty}\spadesuit(\tau)\,d\tau,$$

where the latter approximation is facilitated by $\tau = -\frac{1}{\epsilon} \sim -\infty$ when $t = 0$ for the lower limit. We evaluate this integral asymptotically using a second application of steepest descents, in the variable τ. It is easy to see that

$$\frac{\partial q}{\partial\tau}(\hat{\tau},\bar{\delta}_n) = 0 \quad \text{when } \hat{\tau} = -\frac{\gamma}{\alpha}\bar{\delta}_n$$

for the first two terms in (36). Moreover, $q(\hat{\tau},\bar{\delta}_n) = 0 + O(\epsilon^6)$, which will greatly simplify further evaluation. Expanding the second derivative at the stationary point gives

$$\hat{q}_{\tau\tau}(\hat{\tau}) = -4\epsilon^2\bar{\delta}_n^2\frac{\alpha^2}{\gamma^2}\left(1-4\epsilon^2\bar{\delta}_n^2\frac{\alpha^2}{\gamma^2}\right)+O\big(\epsilon^6\big).$$

Then steepest descents gives

$$\bar{r}_{\text{selection}} \sim \epsilon t_0\left(\frac{\sqrt{2\pi}}{\sqrt{-\hat{q}_{\tau\tau}}}\spadesuit(\tau)\right)\Bigg|^{\tau=\hat{\tau}=-\frac{\gamma}{\alpha}\bar{\delta}_n} = r_0+\epsilon^2\bar{\delta}_n^2\left(4r_0\frac{\alpha^2}{\gamma^2}-\frac{1}{t_0}\right)+O\big(\epsilon^4\big). \quad (37)$$

Now we can return to the UBE, (7), to determine how $\bar{r}_{\text{selection}}$ influences the evolutionary dynamics near r_0.

$$\begin{aligned} r_0+\epsilon^2\frac{1}{t_0}\bar{\delta}_{n+1}^2 = \bar{r}_{n+1} &= \bar{r}_n + h^2[\bar{r}_{\text{selection}}-\bar{r}_n] \\ &= r_0+\epsilon^2\frac{1}{t_0}\bar{\delta}_n^2+h^2\left[r_0+\epsilon^2\bar{\delta}_n^2\left(4r_0\frac{\alpha^2}{\gamma^2}-\frac{1}{t_0}\right)-r_0-\epsilon^2\frac{1}{t_0}\bar{\delta}_n^2\right] \\ &\quad +O\big(\epsilon^4\big). \end{aligned} \quad (38)$$

Simplifying,

$$\bar{\delta}_{n+1}^2 = \left[1 + 2h^2\left(2r_0t_0\frac{\alpha^2}{\gamma^2} - 1\right)\right]\bar{\delta}_n^2 + O\left(\epsilon^2\right). \tag{39}$$

For stability, the term multiplying h^2 must be negative, but larger than $-1/h^2$, or

$$-\frac{1}{h^2} < 2r_0t_0\frac{\alpha^2}{\gamma^2} - 1 < 0.$$

Adding one to both sides gives

$$1 - \frac{1}{h^2} < 2r_0t_0\frac{\alpha^2}{\gamma^2} < 1.$$

Since the heritability, h^2, is always smaller than one while $r_0, t_0 > 0$, the leftmost inequality is always satisfied. The stability requirement becomes

$$r_0t_0\frac{\alpha^2}{\gamma^2} < \frac{1}{2}. \tag{40}$$

The parameter α^2 relates to the curvature of the G function at t_0, and so (40) suggests that the equilibrium distribution will be stable if the G function has sufficiently small curvature at its marginal fixed point. Alternatively, since the distance between the stable and unstable fixed points scales with γ/α, we may expect that the equilibrium distribution will be stable in situations where the fixed points are sufficiently broadly separated.

4 Numerical Results

In this section, we verify the analytical results by solving the model numerically and offer some additional insight into these results. Solving (8) and (14) requires the calculation of $G^{-1}(t, r)$, which cannot be done analytically because G has horizontal and vertical discontinuities (see Fig. 3). The discontinuities in G arise because cold temperatures can arrest development for some life-stages while allowing it to continue for others. The variables r and t are discretized into steps of size Δr and Δt, respectively, typically $\Delta t = 1$ day giving rise to $365/\Delta t + 1$ difference equations to be solved for each year n. In practice, we run simulations for much finer discretisations to ensure that the numerical scheme approximates the integral terms in the model with high accuracy. We developed a numerical scheme that overcomes the difficulties of dealing with discontinuities in G while also being computationally fast. The algorithm is presented in Fig. 3.

Numerical results were obtained using this algorithm with the initial distribution of eggs given by $E_0(t) = 50\exp(-(200-t)^2/(2(50^2))$ and parameter values: $\rho_1 = 0.0055$, $\theta_1 = 9$, $\theta_2 = 11$, $T_0 = 10$, $T_1 = 10$, $k = 2$, $\sigma = 0.0005$, $h^2 = 0.2$, $\Delta r = 0.0001$, $\Delta t = 1/20$ day unless otherwise stated. The parameters are taken from the model system studied by Powell et al. (2000).

Algorithm: Calculating the number of adult emergers.

We wish to calculate $E_n[G^{-1}(t',r)]\Delta t / G_t(t,r)$, the number of adults emerging on day t' of year $n+1$. Let j index the discretisation of t and i index the discretisation of r.

Step 1 Calculate the cumulative distribution of $E_n(t)$, $\text{cum}(E_n(t)) = \int_0^t E_n(s)\,ds$, the total number of eggs laid between day 0 and t. Store $\text{cum}(E_n(t))$ in entry $(i,G(t,r_i))$ of the matrix (M). The ith row of the matrix M contains the total number of adults that have emerged by day $G(t,r_i)$ assuming that all the eggs, $E_n(t)$, have developed at rate r_i.

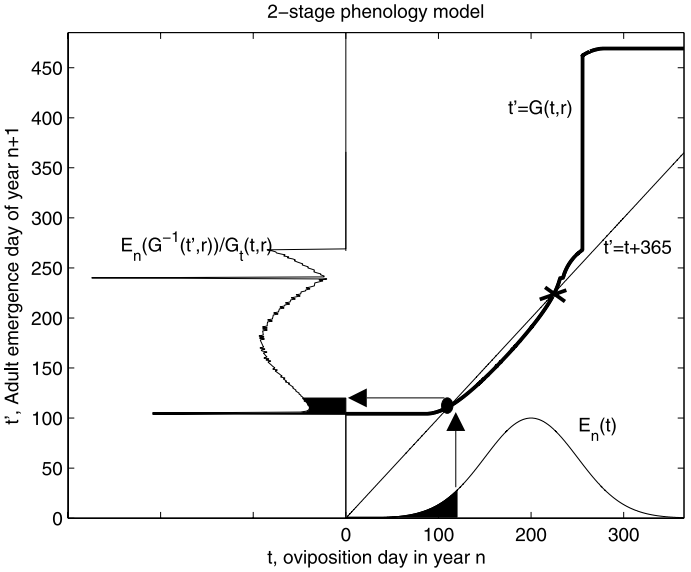

Step 2 Find the total number of adults emerging on each day rather than the cumulative number by taking the difference between consecutive nonzero column elements of M storing the output in the matrix M'.

Step 3 The column index of M' is given by the integers $j = G(t,r) \in (1,\infty)$, where j refers to day $j\Delta t$ of year n. The model assumes 100% mortality for individuals developing either too slowly or too rapidly thus we must truncate the matrix M', keeping only those that emerge in year $n+1$. Columns $365/\Delta t + 1$ through to $730/\Delta t$ correspond to those that emerge in year $n+1$, we remove all other columns. The truncated matrix contains $E_n[G^{-1}(t,r_i)]\frac{\Delta t}{G_t(t,r_i)}$ in entry (i,t).

Step 4 Finally, take into account the fact that only part of the population develop at rate r_i by multiplying row i of M' by $p(r_i)$. Summing over a column t' of this new matrix gives the adult emergence distribution $A_{n+1}(t')$.

Fig. 3 Algorithm: Calculating the number of adult emergers

4.1 Results

Consistent with the analysis of Sect. 3, the numerical results show that the quantitative genetics model slowly converges to an evolutionary fixed point (r_0 and $E_\infty(t)$) (see Fig. 4a, 4b). Figure 1 shows that the underlying phenology model, $t_{i+1} = G(t_i, r_0)$, has a non-generic univoltine fixed point at t_0. As predicted by the theory, the intersection of the G-function with the fixed point line is *tangential* as opposed to transverse; we thus refer to t_0 and the corresponding value of r_0 as a *marginal fixed point*. The emergence distribution, $E_\infty(t)$, resembles a log-normal distribution with mode located at $t = t_0$ as illustrated in Fig. 4b.

A further comparison of the analytical and numerical results is done by explicitly calculating the fixed point of the UBE and finding the corresponding stability condition for the 2-stage phenology model (see Appendix for the analytical derivation). Figure 5a illustrates that the analytical approximation to the fixed point is in good agreement with the numerics over a range of parameters. We see that under a fixed mean yearly temperature, increases in the seasonal fluctuation in yearly temperature

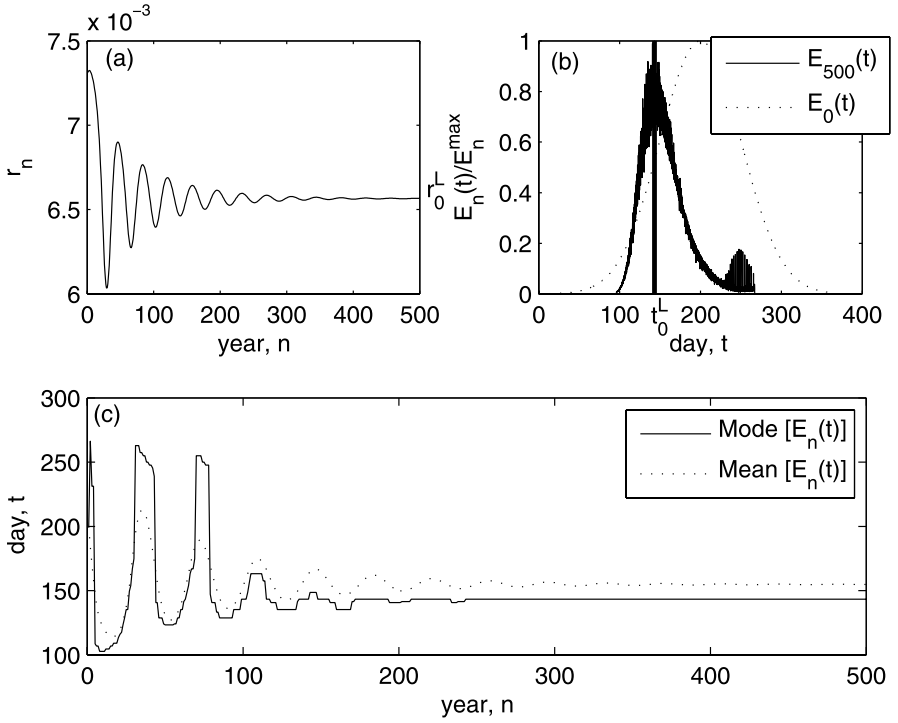

Fig. 4 Using a discretisation of $\Delta t = 1/20$ day and $\Delta r = 0.0001$, (8) and (14) were iterated for $n = 1000$ years allowing model convergence. (**a**) Plot of $\bar{r}_n$ against year n. $\bar{r}_n$ slowly converges to $r_0^L = 0.00657$. (**b**) Plot of the initial and final emergence distribution. The distribution is skewed to the left and t_0^L indicates the location of the mode of $E_\infty(t)$, and is the fixed point of $t_{i+1} = G(t_i, r_0^L)$. The discontinuities in $E_\infty(t)$ are due to the jump discontinuities in G. (**c**) Plot of the mode and mean of $E_n(t)$ as a function of n. The initial value for the mean of r is given by $\bar{r}_0 = 0.0073$, all other parameters are given in the text

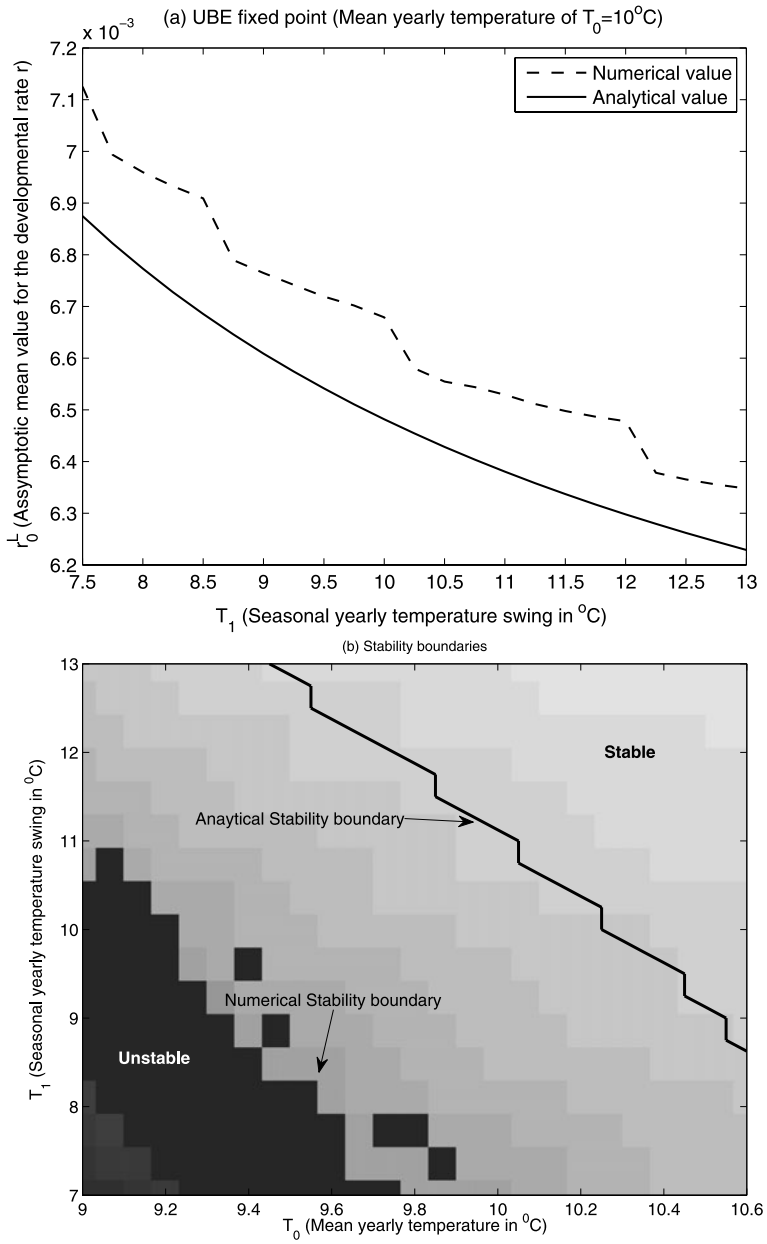

Fig. 5 (**a**) Plot of the numerical value and analytical approximation for r_0^L as a function of seasonal yearly temperature swing. Large temperature swings lead to slower mean developmental rate. (**b**) Numerical and analytical stability boundaries partitioning the T_0–T_1 parameter-space. The dark region indicates unstable dynamics predicted by the numerics and the light region corresponds to stable dynamics. The line indicates the stability boundary predicted by the analysis. High mean temperature and large temperature swings stabilise the evolutionary dynamics. All parameter values are given in the main text. A very fine discretisation of t and r was chosen to ensure that the numerical solution gave a very close approximation to the integral terms in the model, which ensures the numerical boundaries reflect the 'true' model solution

lead to a reduction in r_0. Large seasonal fluctuations favour slower development. In Fig. 5b, we see that large season swings and high mean temperatures also stabilise the evolutionary fixed point.

The two-stage phenology model can have more than two fixed points in some parameter regimes, so we examined the three fixed point case numerically. There are, in fact, two values of r that give rise to marginal fixed points in the parameter regime we have studied, r_0^L (discussed above) and r_0^U. Figure 1 illustrates the phenology model for these two values; r_0^U produces the upper (late year) marginal fixed point and r_0^L produces the lower (early year) marginal fixed point. An upper marginal fixed point exists because the G-function changes shape for large r. Increasing r above r_0^L creates a second stable fixed point (dash-dot line in Fig. 1) when $r = r_c$. A further increase in r changes the timing of the vertical jump discontinuity in G. The vertical jump in G moves to earlier in the year, now occurring before the first horizontal jump discontinuity. This destroys the first stable fixed point and allows the second stable fixed point to become marginal.

Since $t_{i+1} = G(t_i, r)$ can exhibit a marginal fixed point for two values of r, the question then arises to which value does the genetic model converge? The answer to this question depends on σ, the standard deviation of r. For sufficiently large σ, the model converges to the lower marginal fixed point, r_0^L. When σ is small convergence is to the upper marginal fixed point, r_0^U. We now discuss the factors determining convergence to these two marginal fixed points.

4.2 Explaining Marginality and the Emergence Distribution

We begin by discussing the conditions for the convergence to the lower marginal fixed point, r_0^L. Provided $r_0^L < r < r_c$, fixed points, t^*, of $t_{i+1} = G(t_i, r)$ exist and satisfy $t^* < t_0^L$ and are clustered close to t_0^L. However, for $r < r_0^L$, the phenology model ceases to have fixed points and the life-cycle becomes asynchronous, development is slow and emergence occurs after t_0^L. Consequently, a heavy-tailed distribution of emergence times ($E_\infty(t)$) is observed in the model. The asynchronous emergence of slow developers produces the fat tail, while the cluster of fixed points around t_0^L gives rise to the mode of the distribution.

The convergence of $\bar{r}_n$ and $E_n(t)$ is driven by selection and to understand the process we consider $\bar{r}_n$ such that $r_0^L < \bar{r}_n < r_c$. The corresponding emergence distribution, $E_{n+1}(t)$, has a mean to the right of the mode (see Fig. 4c). Since the attracting fixed points are clustered around the mode, t^*, the mass of the emergence distribution which lies to the right of this is attracted to these fixed points, thus the mean emergence time decreases. However, since r is normally distributed in each sub-population (on each day), 50% of the population to the left of the mode will have developmental rates slower than the mean and are attracted toward later emergence. The overall effect of these two processes is a shift in the mode of the emergence distribution to the right, later emergence. Since fitness is defined by per capita growth rate the slower developers become fitter, thus selection acts to reduce $\bar{r}_n$. The tail of the emergence distribution also becomes fatter as a result of the increased number of asynchronous emergers (individuals with $r < r_0^L$) that are created. Figures 6c and d illustrate the

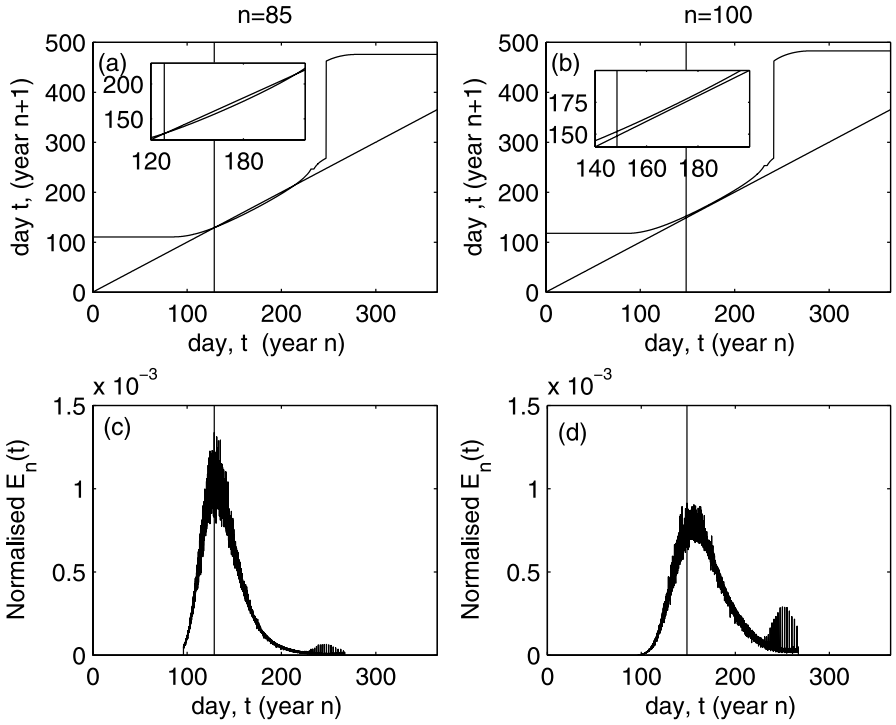

Fig. 6 (**a**) and (**b**) Plots of $t_{i+1} = G(t_i, \bar{r}_n)$, where $n = 85$ and $n = 105$, respectively. A fixed point of G is indicated by the intersection of G with the 45° line. The vertical line in each plot indicates the mode emergence time for the population, and corresponds to the stable fixed point of $t_{i+1} = G(t_i, \bar{r}_n)$ if a fixed point exists. (**c**) and (**d**) Plots of the emergence distribution, $E_n(t)$, where $n = 85$ and $n = 105$, respectively. The distribution is skewed to the left and most individuals emerge after the mode. Thus, fitness of slower developing individuals is increased until as in (**d**) $t_{i+1} = G(t_i, \bar{r}_n)$ no longer has fixed points. The tail of the emergence distribution is caused by slow developers with an asynchronous life cycle, the lack of an attracting fixed point then reduces the fitness of the slower developers and selection acts to increase $\bar{r}_n$. The model parameters are as indicated in the text and $\bar{r}_0 = 0.007$

changes in the emergence distribution and a and b illustrate the G-function for the corresponding value of $\bar{r}_n$, showing the direction of selection.

The strength of the selection we observe is determined by $\bar{r}_{\text{selection}}$ which is an average of r, weighted by $p(r; \bar{r}_n)W_n(r)$. As described above, the per capita growth rate, $W_n(r)$, is largest for small r (Fig. 7c) and provided $W_n(r)$ is large enough that it outweighs the small probability that $r < \bar{r}_n$, selection indeed acts to decrease $\bar{r}_{\text{selection}}$, and hence decrease $\bar{r}_{n+1}$ (see Fig. 7a and c). In each consecutive generation, $\bar{r}_n$ will continue to decrease in this way until $\bar{r}_n < r_0^L$. Once $\bar{r}_n < r_0^L$, the slow developers that previously drove selection are now asynchronous emergers taking more than a year to develop. Without an attracting fixed point, asynchronous emergers rapidly attain a broad distribution of emergence dates thereby lowering the per-capita growth rate of slow developers. Only the subpopulation of fast developers with $r > r_0^L$, and which have an attracting fixed point, show an increase in per capita growth rate, and hence selection acts to now increase $\bar{r}_n$ (see Fig. 7b and d).

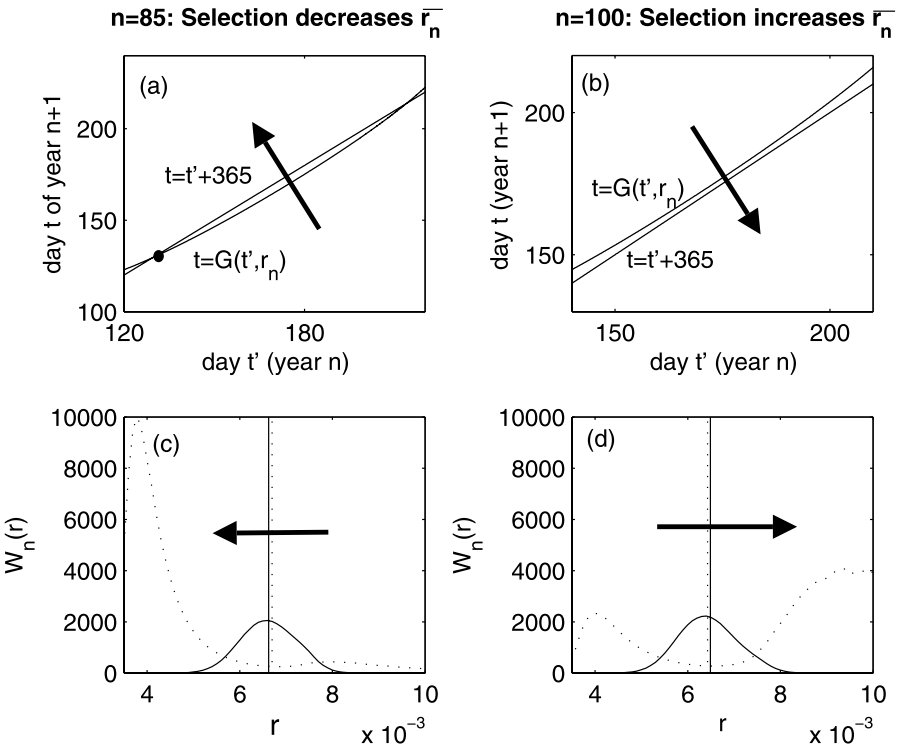

Fig. 7 (**a**) and (**b**) Plots of $G(t, \bar{r}_n)$, where $n = 85$ and $n = 105$, respectively. Selection acts on $\bar{r}_n$ such that G moves in the direction of the arrow, • denotes a stable fixed point of G. (**c**) and (**d**) Plots of the 'fitness' function, $W_n(r)$, against r (*dotted line*). $W_n(r)$ is skewed to the left in (**c**) and to the right in (**d**), reflecting the increased fitness of slow and fast developers, respectively. The *solid curve* is $p(r; \bar{r}_n)W_n(r)0.01$, the mean of this distribution is $\bar{r}_{\text{selection}}$. The *vertical solid line* is located at $\bar{r}_{\text{selection}}$, while the *dashed vertical line* is located at $\bar{r}_n$. The *arrows* indicate the direction of selection. The model parameters are as indicated in the text and $\bar{r}_0 = 0.007$

This is the portion of the numerical experiment which mimics the analytic stability analysis. If the curvature of G ($\sim \alpha^2$) is sufficiently small, there is no overcompensation and convergence occurs without oscillation. However, if α^2 is larger, it is possible for $\bar{r}_{\text{selection}}$ to overshoot r_0, at which point selection acts to decrease $\bar{r}_n$ once more. Over time, these oscillations in $\bar{r}_n$ about r_0^L become smaller in amplitude. The oscillatory convergence of $\bar{r}_n$ to r_0^L is in part a consequence of an intrinsic time lag in the discrete time model. For large n, the emergence distribution, $E_n(t)$, stabilises and approaches an equilibrium distribution and the selective force acting at each generation declines, thus changes in $\bar{r}_n$ become smaller and $\bar{r}_n$ converges to r_0^L.

The type of selection the population undergoes is key to fully understanding the evolutionary processes in this model. Under density- and frequency-*independent* selection, fitness does not change as a function of generation and so the mean trait $\bar{r}_n$ would converge to a fitness maximum (Gomulkiewicz and Holt 1995). In contrast, selection in (8) and (14) is frequency- and density-*dependent*, resulting in $\bar{r}_n$ converging to a fitness minimum of $W_n(r)$ (Fig. 8). Lande (1976) shows how frequency-

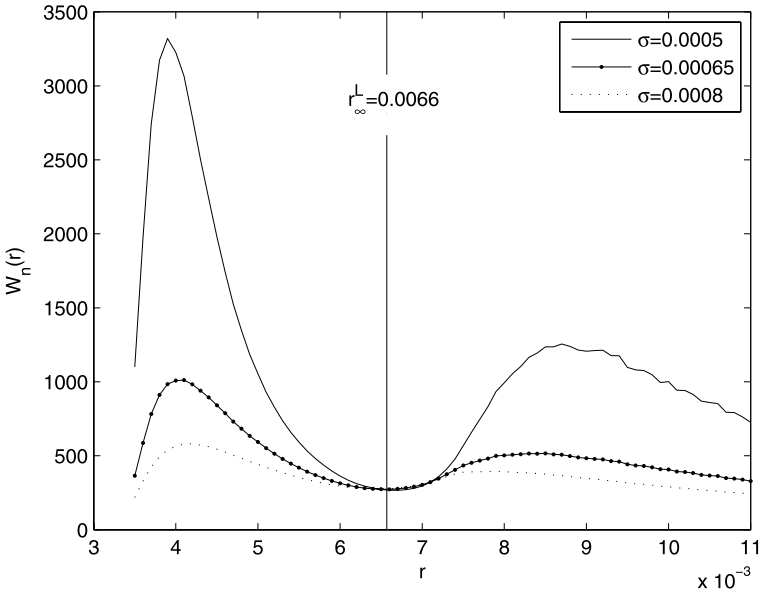

Fig. 8 Plot of the asymptotic 'fitness' function $W_n(r)$ at $n = 1000$ as a function of r. Convergence of $\bar{r}_n$ to r_0^L has occurred by $n = 500$. r_0^L is the location of the fitness minimum for the 3 values of σ considered. Fitness of $r \neq r_0^L$ decreases as a function of σ. When σ is small few individuals in the population have $r \neq r_0^L$ since r is normally distributed in the population the individuals with $r \neq r_0^L$ require an increased fitness to maintain r_0^L as a stable evolutionary fixed point

dependent effects on fitness that do not cancel each other out can produce a maladaptive equilibrium, a mean trait that is not at the fitness maximum. In our case, asymmetry in the emergence distribution selects for some phenotypes (synchronous emergers) over others (asynchronous emergers). So frequency-dependent selection affects traits either side of the mean in different ways. By differentiating the expression for mean fitness ($\bar{W}$) with respect to $\bar{r}_n$, Lande (1976) showed that the change in the average phenotype given by (7) can be reexpressed as follows:

$$\Delta\bar{r}_n = \frac{h^2\sigma^2}{\bar{W}}\left(\frac{\partial\bar{W}}{\partial\bar{r}_n} - \int p(r)\frac{\partial W}{\partial\bar{r}_n}\,dr\right).$$

The first term arises when selection is frequency-independent the second term comes from the frequency-dependent component of selection. Since $W_n(r)$ is not symmetrical about $\bar{r}_n$ we find that the second term is nonzero, and hence selection takes us away from a fitness maximum leading to maladaptation. The clustering of fixed points in the phenology model drives the maladaptation and gives rise to the nonsymmetrical fitness function. In our case, maladaptation manifests itself in the form of asynchrony in the emergence dates for a portion of the population.

An argument analogous to the one above which explains convergence to r_0^L can be used to explain convergence to the upper marginal fixed point, r_0^U, that occurs when the standard deviation in r is small. If the standard deviation in r is large enough,

then $\bar{r}_n$ converges to r_0^L instead. In the next section, we explain in more detail how σ determines the evolutionary end points of the model.

4.3 Convergence Under Small and Large Genetic Variance

The way in which genetic variance determines the evolutionary end points of the genetic model can be understood by considering the global stability of the phenology model. In Fig. 1, we saw that for certain values of r the phenology model has two stable fixed points. The unstable fixed point separating them is located close to the upper stable fixed point. Therefore, the upper stable fixed point has a small basin of attraction. Increasing r reduces the size of this basin of attraction by bringing the upper stable fixed point closer to the unstable fixed point, eventually annihilating both points. In contrast, decreasing r prolongs development, $G(t_i, r)$ increases and the location of the vertical jump discontinuity changes, and the second stable fixed point is lost. Therefore, the upper stable fixed point exists for only a very narrow range of r (e.g. $r \in (0.0073, 0.0078) = (r_c, r_0^U)$) as illustrated in Fig. 1.

The small basin of attraction for r_0^U limits convergence to this fixed point. The quantitative genetics model assumes a normal distribution for r consequently $\bar{r}_n$ converges to r_0^U provided this distribution lies largely inside the basin of attraction for r_0^U. In fact, this is only possible for a limited range of σ ($\sigma < 0.0004$). Following this argument, we expect that large variance in r will always lead to convergence to r_0^L as a significant portion of the population are attracted to fixed points close to t_0^L. What is not clear is why small variance always leads to convergence to r_0^U and is not dependent on the initial conditions. To address this question, we examine the percentage mortality per year under small and large σ (results not shown). For large σ, population loss is negligible and convergence is always to r_0^L. In fact, most of the population loss that occurs is due slow developers, individuals emerging in year $n+2$. For small σ, the years when $\bar{r}_n$ is small are associated with high population loss and depending on parameters, such as h^2, this mortality can either lead to population extinction or a reduction in the per capita growth rate for small r such that selection then acts to increase $\bar{r}_n$ toward r_0^U.

In summary, convergence to the upper marginal fixed point is, in the case of small variance, driven by population loss. As validation, we extended the model framework to allow the possibility of semivoltinism, a 2-year development time, thus preventing the mortality of slow developers. As expected, in the semivoltine model small σ yields convergence to r_0^L or r_0^U depending on initial conditions and population loss becomes negligible (results not shown).

4.4 Stability Boundaries and Extinction Risk

In Sect. 4.3, we found that σ determined the evolutionary end point of the quantitative genetics model. In Fig. 9, we plot the σ–h^2 parameter space showing the stability boundaries separating the evolutionary end points. The heritability, h^2, is the ratio of genetic (σ^2) to total phenotype variance ($\sigma_e^2 + \sigma^2$), and measures the fraction of the phenotype variability which can be passed from one generation to the next; σ_e^2 is the environmental component of the variance. Both h^2 and σ play important roles

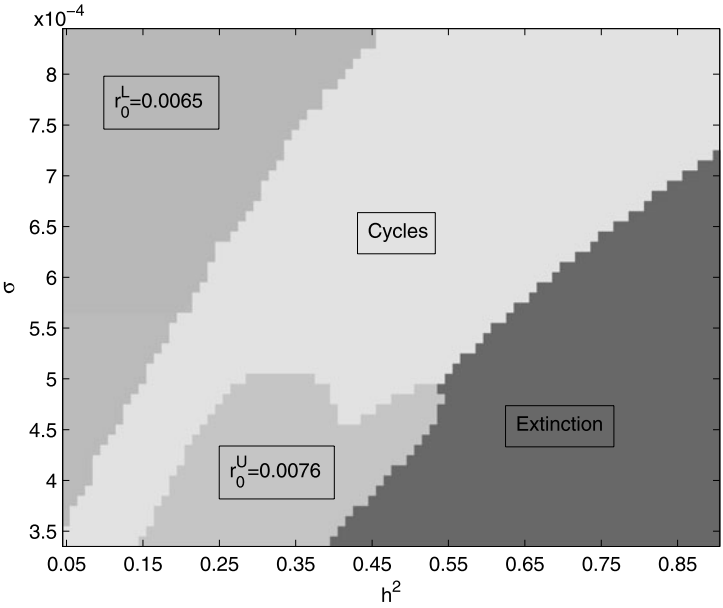

Fig. 9 Numerical stability boundaries partitioning the h^2–σ parameter-space. The region "extinction" indicates a high risk of population extinction as defined by Gomulkiewicz and Holt (1995), populations dropping below $N_c = 10$ were considered to be at risk from demographic extinction. The regions, r_0^L and r_0^U correspond to convergence to the lower and upper marginal fixed point, respectively. Finally, "cycles" denotes regions where $\bar{r}_n$ asymptotes to a stable cycle. Increasing environmental variance increases stability. The parameters are given in the main text

in determining the strength of selection which in turn determines convergence of the model.

In Fig. 9, σ–h^2 parameter space is separated into 4 regions: convergence to r_0^L, convergence to r_0^U, cycles in $\bar{r}_n$, and 'high risk of extinction'. We use the definition of 'high risk of extinction' defined by Gomulkiewicz et al. (1995), below a threshold population size N_c, populations are considered highly vulnerable to extinction, an extinction risk associated with demographic stochasticity. A suggested value of N_c is in the range 10–100, based on theoretical studies (MacArthur and Wilson 1967; Lande 1993). For the purposes of this study, we chose $N_c = 10$.

The region where cycles in $\bar{r}_n$ are observed is a result of the population loss discussed in Sect. 4.3. We see that when $\bar{r}_n$ drops below r_0^L the population mortality in the following year peaks. The large drop in fitness for small r leads to a large increase in $\bar{r}_n$ such that $\bar{r}_n > r_c$. Then population mortality caused by fast developers emerging in year n takes over and drives $\bar{r}_n$ below r_c. This is highlighted by an extreme skewness in the emergence distribution.

Fixing h^2 and increasing σ^2 increases stability of the fixed point of the UBE (Fig. 9). Thus, increases in genetic and environmental variance are stabilising. If instead we fix σ^2 and allow h^2 to increase, we find that stability is lost. Thus, decreasing the environmental variance alone is destabilising.

5 Discussion

There are many models in the literature describing developmental rate curves for insect development (see Roy et al. 2002 for a review). Such models are important components for predicting among other things the synchrony between predator and prey (Logan 2008). Our work has used a quantitative genetics approach to study the evolution of the developmental rate curves that govern phenology. Developmental rate has been shown to be a phenotype that is under genetic selection in a number of insect systems (Taylor 1981). Quantitative genetics is used to evolve the mean phenotype, developmental rate, and the distribution of emergence times. The framework we introduce is very flexible, any choice of phenology model can easily be introduced through choosing an appropriate G-function. Similarly, measured or changing temperature profiles can also be introduced via the same function.

The outcome of the genetic model is convergence to a mean developmental rate corresponding to a marginal fixed point; by this we mean that the mean phenotype corresponds to a marginally stable fixed point of the phenology model. The asymptotic mean phenotype gives rise to synchronised adult emergence with a generation time of one year (univoltinism). However, given that the trait r is normally distributed in the population not all of the population is univoltine. In fact, only the half with a developmental rate greater than the mean will be univoltine and the remainder of the population have a phenotype for which the corresponding phenology model has no such fixed point and this subpopulation has an asynchronous life cycle. The corresponding equilibrium distribution of emergence dates is strongly skewed because the univoltine fixed points focus the asymptotic emergence distribution about the mode (the fixed point of $t_{i+1} = G(r_0^L, t_i)$), and the asynchronous subpopulation gives the fat tails of the distribution. The tails in the emergence distribution could be important for a population in a changing environment in which the evolutionary fixed point r_0^L will change with the environment (e.g. yearly temperature). Individuals emerging later in the year could also provide a buffer against rare catastrophic events that could otherwise extinguish a population if the emergence dates were too tightly grouped.

Although we have focussed on the evolution of the developmental rate of an insect feeding stage, evolution of other rate curve parameters such as ρ_1 and the developmental thresholds, θ_1 and θ_2, can easily be studied in the framework we have presented. Numerical results show that evolution of these parameters also give rise to the same evolutionary end point, a marginal fixed point. The thresholds, θ_1 and θ_2 are tightly coupled to the yearly temperature fluctuations so evolution in these parameters readily leads to a switching in the location of the jump discontinuities in the phenology model and evolutionary cycles in the phenotype become more common (see Sect. 4.4). The presence of stable cycles in $\bar{r}_n$ are driven by population loss and once semivoltinism is accounted for the loss driving the oscillations is removed, so the oscillations decrease in amplitude. Hypotheses have connected such fluctuating selection to rapid evolution, thus oscillations in phenotype may be an observable phenomenon (Thompson 1998).

Preliminary work indicates that the predicted evolutionary end point for developmental rates is unchanged by a changing temperature environment. The evolutionary dynamics are able to track the moving location of the marginal fixed point of the

G-function. The synchronising force provided by the fixed points in the phenology model is key to the frequency-dependent selection which drives evolution to the marginal fixed point. The study by Powell and Logan (2005) examined a phenology model using historic temperature profiles and a fully parameterised 8-stage life-cycle model for the mountain pine beetle and they found the basic properties of the G-function that drive evolution in our model continue to hold. Specifically the G-function has a stable-unstable pair of fixed points with small curvature around these fixed points. So this is strong evidence to expect the marginal fixed point to be the evolutionary end point in more biologically realistic models of insect development than the caricature studied here. The effect of changing temperature profiles and other phenology models is the subject of future work.

While it is difficult to experimentally estimate the evolutionary rates that the model predicts, as they rely on knowing the heritability of the trait, h^2, the model does suggest slow adaptation and rapid synchronisation in the two life-stage model (see Appendix). For the mountain pine beetle system, Bentz et al. (2001) have found evidence for strong local selection for median developmental time among geographically separated populations. Slower development was found in southern populations, where temperatures are warmer, and faster development was seen in northern populations. This is consistent with our model predictions whereby selection acts to maintain univoltism in each temperature environment.

The quantitative genetics approach we have used to study evolution of phenology is robust to many of the model assumptions and can be easily generalised to include alternative phenology models and more complicated reproduction and selection functions. Moreover, it is possible to attain analytical results which further our understanding. Synchronisation of emergence is a key factor driving selection, however, evolution to a marginal fixed point and corresponding skewed distribution allows asynchronous emergers to persist in the population. Empirical results have shown reproductive asynchrony increases in a population when environments are unpredictable; asynchrony is a risk-spreading strategy and can be advantageous at high population densities (Calabrese and Fagan 2004). At low population densities, asynchrony may be detrimental, but by evolving to a marginal fixed point adaptation to changes in temperature regimes becomes possible. Increases in mean yearly temperature have the effect of accelerating development allowing previously asynchronous emergers to attain a univoltine life-cycle. A trait distribution with a mean corresponding to a marginal fixed point is then well adapted to cope with warming environments.

There are a number of examples of shifts in phenology induced by climate change, for instance, hatch date in insects and spawning date in frogs and toads (Visser 2008). An understanding of the evolution of phenology can offer important insights into the process of adaptation. Visser (2008) argues that phenotypic plasticity will not be adaptive under climate change and microevolution is necessary for adaptation. There is growing evidence that evolution is occurring on ecological timescales for a number of insect species (Skelly et al. 2007), Yamanaka and coworkers found that the webworm, *Hyphantria cunea* Drury, had undergone evolution in life history traits that relate to phenology over a period of just 30 years (Yamanaka et al. 2008). Mechanistic understanding of these processes will become increasingly important as extreme environmental changes become more common.

Acknowledgements Part of this work was carried out during a visit by JP and was supported by the Royal Society. We also thank Brian Yurk for helpful discussions during the early stages of this work.

Appendix: Fixed Points and Stability for the Two-Stage Model

Returning to the two-stage model, we determine the location of the parameters which generate the marginally stable univoltine fixed points selected by the evolutionary dynamics. We will assume that thresholds are selected so that the quiescent developmental period occurs (i.e. temperatures dipping below developmental thresholds) during the second-life stage, but that the first life stage completes development while temperatures are above its threshold, θ_1. We make these assumptions because, firstly, in terms of the evolutionary dynamics this is the steady state with the largest basin of attraction, and secondly, this turns out to be the steady state with emergence occurring at an appropriate season, that is, 'summer.' The other possible steady states can be calculated using similar methods.

Let t_0^n denote the median time of initial oviposition in year n . Then the median time of egg-hatching, t_1, satisfies

$$\begin{aligned} 1 &= \int_{t_0^n}^{t_1} \rho_1 \left[T_0 - T_1 \cos\left(\frac{2\pi t}{365}\right) - \theta_1 \right] dt \\ &= \rho_1 \left[(T_0 - \theta_1)\left(t_1 - t_0^n\right) - T_1 \frac{365}{2\pi} \left(\sin\left(\frac{2\pi t_1}{365}\right) - \sin\left(\frac{2\pi t_0^n}{365}\right) \right) \right]. \end{aligned} \tag{A.1}$$

The emergence time for stage 2 satisfies a much simpler relation,

$$1 = r[t_2 - t_1 - \Delta_2], \tag{A.2}$$

where Δ_2 is the amount of time spent with temperatures below threshold,

$$\frac{1}{2}\Delta_2 = \frac{365}{2\pi} \cos^{-1}\left(\frac{T_0 - \theta_2}{T_1}\right). \tag{A.3}$$

This gives an expression for t_2 in terms of t_1,

$$t_2 = \frac{1}{r} + t_1 + \frac{365}{\pi} \cos^{-1}\left(\frac{T_0 - \theta_2}{T_1}\right). \tag{A.4}$$

Equation (A.1) defines an implicit function, $t_1(t_0^n)$, and using (A.4) we can, in principle, define the G function

$$G\left(t_0^n\right) = t_2\left[t_1\left(t_0^n\right)\right]. \tag{A.5}$$

The condition for marginality is that

$$1 = \frac{dG}{dt_0^n} = \frac{dt_2}{dt_1}\frac{dt_1}{dt_0^n}, \tag{A.6}$$

and since $\frac{dt_2}{dt_1} = 1$ from (A.4), we have

$$\frac{dt_1}{dt_0^n} = 1. \tag{A.7}$$

The derivative of $t_1(t_0^n)$ can be found implicitly from (A.1), which gives

$$0 = \frac{dt_1}{dt_0^n}\rho_1\left[T_0 - T_1\cos\left(\frac{2\pi t_1}{365}\right) - \theta_1\right] - \rho_1\left[T_0 - T_1\cos\left(\frac{2\pi t_0^n}{365}\right) - \theta_1\right]. \tag{A.8}$$

Thus,

$$\frac{dt_1}{dt_0^n} = \frac{T_0 - T_1\cos\left(\frac{2\pi t_0^n}{365}\right) - \theta_1}{T_0 - T_1\cos\left(\frac{2\pi t_1}{365}\right) - \theta_1}. \tag{A.9}$$

Requiring $\frac{dt_1}{dt_0^n} = 1$ gives

$$\cos\left(\frac{2\pi t_0^n}{365}\right) = \cos\left(\frac{2\pi t_1}{365}\right). \tag{A.10}$$

Since only one quiescent period is possible per life stage in a year (given the simple sinusoidal temperature cycle), this gives

$$t_1 = 365 - t_0^n. \tag{A.11}$$

Finally, for the solution to be univoltine, we require

$$t_2 = 365 + t_0^n. \tag{A.12}$$

Taken together, (A.1), (A.4), (A.11), (A.12) determine t_0^n, t_1, t_2 and the equilibrium state for the parameter under evolution, r.

To determine an explicit expression for t_0 and r_0 (the marginal oviposition date and marginal parameter value, respectively, in this case t_0^n and r at equilibrium), we note that (A.11) defines $\sin(\frac{2\pi t_0^n}{365}) = -\sin(\frac{2\pi t_1}{365})$. Then (A.1) defines t_0 implicitly;

$$\frac{1}{\rho_1} = (T_0 - \theta_1)(365 - 2t_0) + T_1\frac{365}{\pi}\sin\left(\frac{2\pi t_0}{365}\right). \tag{A.13}$$

The marginal value for r, (the fixed point r_0), can then be calculated from (A.4),

$$\frac{1}{r_0} = 2t_0 - \frac{365}{\pi}\cos^{-1}\left(\frac{T_0 - \theta_2}{T_1}\right). \tag{A.14}$$

Now we are in a position to calculate the additional parameters required for the stability analysis above. Referring to the quadratic approximation (28), we note

$$\alpha^2 = \frac{1}{2}t_0 G_{tt}(t_0, r_0) \quad \text{and} \quad \gamma^2 = -\frac{1}{(t_0)^2}\frac{\partial}{\partial r}G(t_0, r_0).$$

For α^2,

$$\alpha^2 = \frac{1}{2}t_0 G_{tt}(t_0, r_0) = \frac{1}{2}t_0\left[\frac{d^2t_2}{d(t_1)^2}\left(\frac{dt_1}{dt_0^n}\right)^2 + \frac{dt_2}{dt_1}\frac{d^2t_1}{d(t_0^n)^2}\right],$$

and using $\frac{dt_1}{dt_0^n} = 1$ and $\frac{d^2t_2}{d(t_1)^2} = 0$ from (A.4), we find

$$\alpha^2 = \frac{1}{2}t_0\left\{\frac{T_1\frac{2\pi}{365}\sin\left(\frac{2\pi t_0^n}{365}\right)\left[T_0 - T_1\cos\left(\frac{2\pi t_1}{365}\right) - \theta_1\right]}{\left[T_0 - T_1\cos\left(\frac{2\pi t_0^n}{365}\right) - \theta_1\right]^2}\right.$$
$$\left. - \frac{T_1\frac{dt_1}{dt_0^n}\frac{2\pi}{365}\sin\left(\frac{2\pi t_1}{365}\right)\left[T_0 - T_1\cos\left(\frac{2\pi t_0^n}{365}\right) - \theta_1\right]}{\left[T_0 - T_1\cos\left(\frac{2\pi t_0^n}{365}\right) - \theta_1\right]^2}\right\}.$$

Using (A.11) and $\frac{dt_1}{dt_0^n} = 1$, this simplifies to

$$\alpha^2 = \frac{2t_0\pi T_1}{365}\frac{\sin\left(\frac{2\pi t_0}{365}\right)}{T_0 - T_1\cos\left(\frac{2\pi t_0}{365}\right) - \theta_1}. \tag{A.15}$$

The situation is much simpler for γ^2. Since G depends on the evolution parameter, r, only in the last stage, we can write

$$\frac{\partial G}{\partial r} = -\frac{1}{r^2}.$$

Consequently,

$$\gamma^2 = \frac{1}{r_0^2(t_0)^2}. \tag{A.16}$$

In the particular case of $T_0 = 10, T_1 = 10, \theta_1 = 9, \theta_2 = 11$, and $\rho_1 = 0.0055$ this gives $r_0 = 0.00648$, $\gamma = 0.886$, $\alpha = 0.626$, and $t_0 = 174.21$, in excellent agreement with the numerical solution. Letting $\sigma = 5 \times 10^{-4}$ gives $\epsilon = 0.0871$ in the stability analysis.

References

Bentz, B. J., Logan, J. A., & Vandygriff, J. C. (2001). Latitudinal variation in dendroctonus ponderosae (coleoptera: Scolytidae) development time and adult size. *Can. Entomol.*, *133*(3), 375–387.

Calabrese, J. M., & Fagan, W. F. (2004). Lost in time, lonely, and single: reproductive asynchrony and the Allee effect. *Am. Nat.*, *164*(1), 25–37.

Chesson, P., & Huntly, N. (1997). The roles of harsh and fluctuating conditions in the dynamics of ecological communities. *Am. Nat.*, *150*(5), 519–553.

Danks, H. V. (1987). *Monograph series, No. 1. Insect dormancy: An ecological perspective*. Ottawa: Biological Survey of Canada (Terrestrial Arthropods).

Gilbert, E., Powell, J. A., Logan, J. A., & Bentz, B. J. (2004). Comparison of three models predicting developmental milestones given environmental and individual variation. *Bull. Math. Biol.*, *66*, 1821–1850.

Gomulkiewicz, R., & Holt, R. D. (1995). When does evolution by natural selection prevent extinction. *Evolution*, *49*(1), 201–207.

Hendry, A. P., Wenburg, J. K., Bentzen, P., Volk, E. C., & Quinn, T. P. (2000). Rapid evolution of reproductive isolation in the wild: Evidence from introduced salmon. *Science*, *290*(5491), 516–518.

Holt, R. D. (1990). The microevolutionary consequences of climate change. *Trends Ecol. Evol.*, *5*(9), 311–315.

Jenkins, J. L., Powell, J. A., Logan, J. A., & Bentz, B. J. (2001). Low seasonal temperatures promote life cycle synchronization. *Bull. Math. Biol.*, *63*, 573–595.

Johnson, M. T. J., & Agrawal, A. A. (2003). The ecological play of predator-prey dynamics in an evolutionary theatre. *Trends Ecol. Evol.*, *18*(11), 549–551.

Lande, R. (1976). Natural selection and random genetic drift in phenotypic evolution. *Evolution*, *30*, 314–334.

Lande, R. (1993). Risks of population extinction from demographic and environmental stochasticity and random catastrophes. *Am. Nat.*, *142*, 911–927.

Logan, J. A., Regniere, J., & Powell, J. A. (2003). Assessing the impacts of global warming on forest pest dynamics. *Front. Ecol. Environ.*, *1*(3), 130–137.

Logan, J. D. (2008). Phenologically-structured predator-prey dynamics with temperature dependence. *Bull. Math. Biol.*, *70*(1), 1–20.

Lynch, M., & Lande, R. (1993). Evolution and extinction in response to environmental change. In P. M. Kareiva, J. G. Kingsolver, & R. B. Huey (Eds.), *Biotic interactions and global change* (pp. 234–250). Sunderland: Sinauer Associates.

MacArthur, R. H., & Wilson, E. O. (1967). *Island biogeography*. Princeton: Princeton University Press.

Powell, J. A., & Logan, J. A. (2005). Insect seasonality: Circle map analysis of temperature-driven life cycles. *Theor. Popul. Biol.*, *67*(3), 161–179.

Powell, J. A., Jenkins, J. L., Logan, J. A., & Bentz, B. J. (2000). Seasonal temperature alone can synchronise life cycles. *Bull. Math. Biol.*, *62*, 977–998.

Reznick, D. N., & Ghalambor, C. K. (2001). The population ecology of contemporary adaptations: What empirical studies reveal about the conditions that promote adaptive evolution. *Genetica*, *112*, 183–198.

Roy, M., Brodeur, J., & Cloutier, C. (2002). Relationship between temperature and developmental rate of *stethorus punctillum* (coleoptera: Coccinellidae) and its prey *tetranychus mcdanieli* (acarina: Tetranychidae). *Environ. Entomol.*, *31*(1), 177–187.

Skelly, D. K., Joseph, L. N., Possingham, H. P., Freidenburg, L. K., Farrugia, T. J., Kinnison, M. T., & Hendry, A. P. (2007). Evolutionary responses to climate change. *Conserv. Biol.*, *21*(5), 1353–1355.

Slatkin, M. (1980). Ecological character displacement. *Ecology*, *61*(1), 163–177.

Taylor, F. (1981). Ecology and evolution of physiological time in insects. *Am. Nat.*, *117*(1), 1–23.

Thomas, C. D., Cameron, A., Green, R. E., Bakkenes, M., Beaumont, L. J., Collingham, Y. C., Erasmus, F. N., Ferreira de Siqueira, M., Grainger, A., Hannah, L., Hughes, L., Huntly, B., van Jaarsveld, A. S., Midgley, G. F., Miles, L., Ortega-Huerta, M. A., Townsend Peterson, A., Phillips, O. L., & Williams, S. E. (2004). Extinction risk from climate change. *Nature*, *427*(6970), 145–148.

Thompson, J. N. (1998). Rapid evolution as an ecological process. *Trends Ecol. Evol.*, *13*(8), 329–332.

Visser, M. E. (2008). Keeping up with a warming world; assessing the rate of adaptation to climate change. *Proc. R. Soc., Ser. B*, *275*, 649–659.

Yamanaka, T., Tatsuki, S., & Shimada, M. (2008). Adaptation to the new land or effect of global warming? An age-structured model for rapid voltinism change in an alien lepidopteran pest. *J. Anim. Ecol.*, *77*, 585–596.

Zaslavski, V. A. (1996). Essentials of the environmental control of insect seasonality as reference points for comparative studies in other invertebrates. *Hydrobiologia*, *320*, 123–130.